# Quadruplex Nanostructures of d(TGGGGT): Influence of Sodium and Potassium Ions

**ARTICLE** *in* ANALYTICAL CHEMISTRY · MAY 2014

Impact Factor: 5.64 · DOI: 10.1021/ac500624z · Source: PubMed



**4 AUTHORS:**

Ana Dora Pontinha
University of Coimbra
**13** PUBLICATIONS **70** CITATIONS
SEE PROFILE

AMC Paquim
University of Coimbra
**43** PUBLICATIONS **736** CITATIONS
SEE PROFILE

Ramon Eritja
Spanish National Research Council
**376** PUBLICATIONS **7,034** CITATIONS
SEE PROFILE

Ana Maria Oliveira-Brett
University of Coimbra
**233** PUBLICATIONS **5,154** CITATIONS
SEE PROFILE

analytical chemistry

Article

pubs.acs.org/ac

# Quadruplex Nanostructures of d(TGGGGT): Influence of Sodium and Potassium Ions

Ana Dora Rodrigues Pontinha,[†] Ana-Maria Chiorcea-Paquim,[†] Ramon Eritja,[‡] and Ana Maria Oliveira-Brett*[,†]

[†]Department of Chemistry, University of Coimbra, 3004-535 Coimbra, Portugal

[‡]Institute of Advanced Chemistry of Catalonia (IQAC−CSIC), CIBER-BBN Networking Research Centre on Bioengineering, Biomaterials and Nanomedicine, Jordi Girona 18-26, 08034 Barcelona, Spain

**ABSTRACT:** The *Tetrahymena* telomeric repeat sequence d(TG$_4$T) contains only guanine (G) and thymine (T) bases and has medical and nanotechnological applications because of its ability to self-assemble into stiff tetra-molecular parallel-stranded G-quadruplexes. The hexadeoxynucleotide d(TG$_4$T) was studied using atomic force microscopy (AFM) on the highly oriented pyrolytic graphite surface and differential pulse (DP) voltammetry at a glassy carbon electrode. The d(TG$_4$T) single-strands self-assembled into G-quadruplex structures, very fast in $K^+$ ions solution and slowly in $Na^+$ ions containing solution. The G-quadruplex structures were detected in AFM by the adsorption of small spherical aggregates and by DP voltammetry by the G oxidation peak decrease and G-quartets oxidation peak occurrence, in a time and $K^+$ ions concentration dependent manner. In the presence of $Na^+$ ions, the d(TG$_4$T) single-strands also slowly self-assembled into higher-order nanostructures, detected by AFM as short nanowires and nanostructured films that were never observed in $K^+$ ions containing solution.

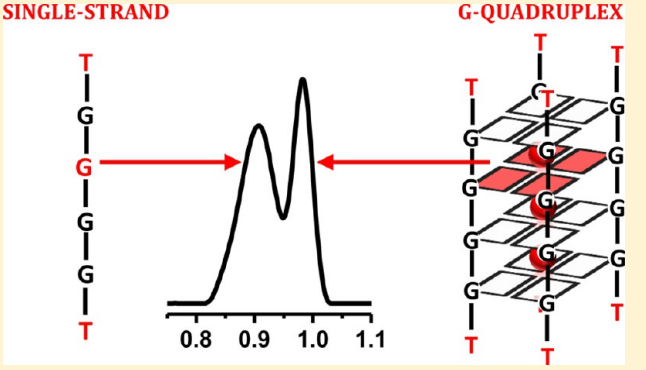


The telomeric ends of chromosomes contain stretches of guanine (G)-rich sequences that can form a variety of four-stranded nucleic acid secondary structures named G-quadruplexes.[1−6] G-quadruplexes are very polymorphic, being classified in terms of their molecularity (the number of associated strands, leading to the formation of monomer, dimer or tetramer G-quadruplexes), the strand polarity (the relative arrangement of adjacent strands in parallel or antiparallel orientations), the glycosidic torsion angle (anti or syn), and the orientation of the connecting loops (lateral, diagonal or both).[2,7−9] Telomeric G-quadruplexes are known to have important roles in chromosome replication, gene regulation and meiosis, their formation increasing the genomic instability by impeding the recognition of the telomeric DNA-associated proteins and impeding the telomerase association and activity.

The hexadeoxynucleotide d(TG$_4$T) is a *Tetrahymena* telomeric repeat sequence, containing only guanine (G) and thymine (T) bases, that forms tetra-molecular G-quadruplex structures (Scheme 1A) in the presence of $Na^+$ and $K^+$ ions in solution.[10−16] The d(TG$_4$T) tetra-molecular quadruplexes present all strands parallel, with all the guanines residues in anticonformation, forming right-handed helical structures with four equivalent grooves.

The G-quadruplexes are built by planar association of four G bases held together by eight Hoogsteen hydrogen bonds, named G-quartets ($G_q$) (Scheme 1B), stack on top of each other by $\pi-\pi$ hydrophobic interactions. The cations are located in between the G-quartet planes, and form cation-dipole interactions with the 8 G of the two adjacent G-quartets, enhancing the hydrogen bond strength and stabilizing the G-quartet staking.

**Scheme 1. Schematic Representation: (A) Tetra-Molecular Parallel-Stranded d(TG$_4$T) Quadruplex and (B) G-Quartet**

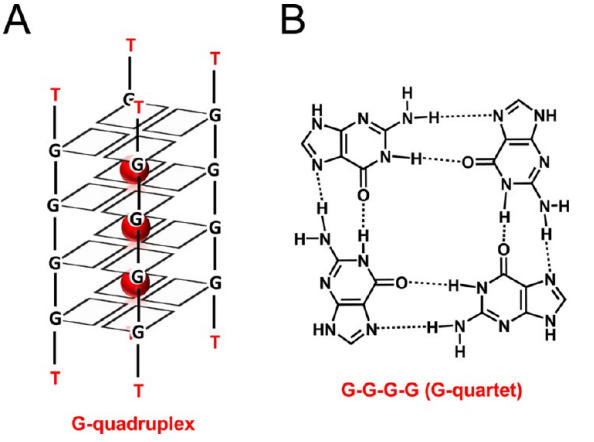


**Received:** February 14, 2014
**Accepted:** May 4, 2014





dx.doi.org/10.1021/ac500624z | *Anal. Chem.* XXXX, XXX, XXX−XXX

The d($TG_4T$) quadruplexes are considered simpler models of biologically relevant G-quadruplexes, being used to obtain high resolution data on drug−DNA interactions.[17−19] The well-known conformation of the d($TG_4T$) quadruplexes and their extraordinary stiffness have made the d($TG_4T$) molecules to be considered good building blocks candidates for the development of novel devices, with medical and nanotechnology applications. In this context, a comprehensive knowledge of the d($TG_4T$) structural and folding properties on the surface of conducting materials is important.

Atomic force microscopy (AFM) is capable of characterizing features at nanoscale and can be used to image biomolecules at single-molecular level, in air or in liquid. Although AFM was used to obtain images of G-quadruplex self-assembled at insulating, hydrophilic mica surfaces[20−22] and more recently at highly oriented pyrolytic graphite (HOPG),[23−28] the investigation of the tetra-molecular parallel-stranded d($TG_4T$) quadruplex formation and its adsorption and stability on the surface of conducting hydrophobic carbon electrodes has not been studied and is relevant from the point view of nanotechnology and biosensor technology applications.

Differential pulse (DP) voltammetry is a powerful method that presents very high sensitivity and selectivity and can be successfully employed for the rapid detection of single-stranded oligonucleotides structural modifications into G-quadruplexes.[8,23−28]

This paper describes a systematic study performed by AFM on the surface of HOPG and DP voltammetry at a glassy carbon electrode (GCE), to elucidate the adsorption mechanism and the redox behavior of the d($TG_4T$) *Tetrahymena* telomeric sequence, with respect to its ability to form G-quadruplex secondary structures and higher-order nanostructures, influenced by the presence of $Na^+$ or $K^+$ ions.

## MATERIALS AND METHODS

**Reagents.** The 10-mer single-stranded d($TG_4T$) hexadeoxyribonucleotides with the base sequence 5′-TGGGGT-3′ were synthesized on an Applied Biosystems 380B automated DNA synthesizer (USA) using reagents for oligodeoxyribonucleotides chemistry purchased from Fluka (Germany). The purity of the d($TG_4T$) sequences was verified by NMR and HPLC analysis.

Microvolumes were measured using EP-10 and EP-100 Plus Motorized Microliter Pipettes (Rainin Instruments Co. Inc., Woburn, U.S.A.). The pH measurements were carried out with a GLP 21 Crison pH meter.

The 0.1 M phosphate buffer pH = 7.0 ($NaH_2PO_4$/$Na_2HPO_4$) supporting electrolyte solution was prepared using analytical grade reagents and purified water from a Millipore Milli-Q system (conductivity <0.1 $\mu S\ cm^{-1}$). Solutions of different concentrations were obtained by direct dilution of the appropriate volume in buffer electrolyte.

**Atomic Force Microscopy.** HOPG, grade ZYB of 15 × 15 × 2 $mm^3$ dimensions, from Advanced Ceramics Co., U.S.A., was used as a substrate in the AFM study. The HOPG was freshly cleaved with adhesive tape prior to each experiment and imaged by AFM to establish its cleanliness. The HOPG surface was used as a substrate in the AFM study, because is atomically flat with less than 0.06 nm of root-mean-square (rms) roughness for a 1000 × 1000 $nm^2$ surface area, while the GCE used for the voltammetric characterization is much rougher, with 2.10 nm rms roughness for the same surface area, therefore unsuitable for AFM surface characterization. HOPG and GCE are $sp^2$ carbon materials, with the exposed defect sites terminated by carbon−oxygen functionalities and electrochemical experiments showed similar redox behavior using GCE and HOPG carbon materials. The GCE structure shows randomly intertwined ribbons of graphitic planes, and the adsorption of molecules on the GCE surface will present similarities with the adsorption at the HOPG edge defects.[29,30]

AFM was performed in the acoustic AC (AAC) mode, with a PicoScan controller from Agilent Technologies, Tempe, AZ, USA. All the AFM experiments were performed with a CS AFM S scanner with a scan range of 6 $\mu$m in $x-y$ and 2 $\mu$m in $z$, from Agilent Technologies. AppNano type FORT of 225 $\mu$m length, 3.0 N $m^{-1}$ spring constants and 47−76 kHz resonant frequencies (Applied NanoStructures, Inc., U.S.A.) were used. All AFM images were topographical and were taken with 256 samples/line × 256 lines and scan rates of 0.8−2.5 lines $s^{-1}$. When necessary, the AFM images were processed by flattening to remove the background slope and contrast and brightness were adjusted.

**Sample Preparation for AFM.** Solutions of 0.3 $\mu$M d($TG_4T$) were prepared in 0.1 M phosphate buffer pH = 7.0 and incubated in the absence or presence of 100 mM KCl, during 0, 24, and 48 h and several days, at room temperature.

The d($TG_4T$) modified HOPG surfaces were obtained by spontaneous adsorption, after depositing 200 $\mu$L of the appropriate d($TG_4T$) solution onto the freshly cleaved HOPG surface, during 3 min. The excess of solution was gently cleaned with a jet of Millipore Milli-Q water, and the HOPG with adsorbed d($TG_4T$) molecules was then dried in a $N_2$ sterile atmosphere and imaged by AAC Mode AFM in air.

**Voltammetric Parameters and Electrochemical Cells.** Voltammetric experiments were carried out using a $\mu$Autolab Type III potentiostat running with GPES 4.9 software (Metrohm-Autolab, Utrecht, the Netherlands). The experimental conditions for DP voltammetry were pulse amplitude 50 mV, pulse width 70 ms, and scan rate 5 mV $s^{-1}$. Measurements were carried out using a a glassy carbon working electrode (GCE) ($d$ = 1 mm), a Pt wire counter electrode, and an Ag/AgCl (3 M KCl) reference electrode, in a one-compartment 3 mL electrochemical cell (Echem Electrode Kit, eDAQ Products, Poland).

The GCE was polished using diamond spray (particle size 1 $\mu$m, Kemet International Ltd., UK) before every electrochemical assay. After polishing, the electrode was rinsed thoroughly with Milli-Q water. Following this mechanical treatment, the GCE was placed in buffer supporting electrolyte and various DP voltammograms were recorded until a steady state baseline voltammogram was obtained. This procedure ensured very reproducible experimental results.

**Acquisition and Presentation of Voltammetric Data.** DP voltammograms were baseline corrected using the moving average with a step window of 2 mV included in GPES version 4.9 software. This mathematical treatment improves the visualization and identification of peaks over the baseline without introducing any artifact, although the peak height is in some cases reduced (<10%) relative to that of the untreated curve. Nevertheless, this mathematical treatment of the original voltammograms was used in the presentation of all experimental voltammograms for a better and clearer identification of the peaks. The values for peak current presented in all graphs were determined from the original untreated voltammograms after subtraction of the baseline.


dx.doi.org/10.1021/ac500624z | *Anal. Chem.* XXXX, XXX, XXX−XXX

## RESULTS

**AFM Characterization.** The capacity of d($TG_4T$) to interact and adsorb spontaneously on the HOPG surface, forming different morphological films, was investigated by AFM, using solutions of 0.3 $\mu$M d($TG_4T$) in 0.1 M sodium phosphate buffer pH = 7.0.

AFM images of d($TG_4T$) spontaneously adsorbed from freshly prepared solutions (0 h incubation) showed only randomly oriented polymeric structures (rP − random polymer, Figure 1A) of 0.89 ± 0.1 nm height because of the adsorption of single-stranded d($TG_4T$) molecules. AFM images of d($TG_4T$) obtained after 24 h incubation showed a similar adsorption pattern.

AFM images after 48 h incubation (Figure 1B) showed three adsorption morphologies: (i) rP randomly oriented polymeric structures and network films of 0.81 ± 0.1 nm height because of the adsorption of d($TG_4T$) single-strands, (ii) spherical aggregates (A, aggregates) of 2.15 ± 0.6 nm height because of the adsorption of short tetra-molecular d($TG_4T$) quadruplexes and sporadically (iii) short nanowires (N, nanowire, Figure 1B inset) of 0.80 ± 0.1 nm height and length up to 100 nm.

AFM images after 7 days incubation (Figures 1C) also showed three adsorption morphologies: (i) very rarely, rP randomly oriented polymeric structures and network films of 0.81 ± 0.1 nm height becaues of the adsorption of d($TG_4T$) single-strands, (ii) A spherical aggregates of 2.05 ± 0.5 nm height because of the adsorption of d($TG_4T$) quadruplexes, close to the G-quadruplex diameter of ~2.8 nm measured by X-ray crystallography,[31,32] and (iii) oriented polymeric domains (oP, oriented polymer) of 0.81 ± 0.1 nm height, adsorbed along one of the three axes of symmetry of the HOPG basal planes.

To establish the influence of the presence of $K^+$ ions in the formation and stabilization of d($TG_4T$) quadruplexes, the adsorption of d($TG_4T$) after incubation with 100 mM $K^+$ ions during different periods of time was also investigated.

AFM images of d($TG_4T$) immediately after the addition of $K^+$ ions (Figure 2A, 0 h incubation) showed two adsorption morphologies: (i) rP randomly oriented polymeric structures of 0.71 ± 0.2 nm height, due the adsorption of d($TG_4T$) single-strands and (ii) A spherical aggregates of 1.87 ± 0.4 nm height, due to the adsorption of d($TG_4T$) quadruplexes. Increasing the incubation time to 24 h, 48 h (Figure 2B), 72 h and 7 days incubation (Figure 2C), the number of 1.85 ± 0.5 nm height A aggregates increased, while the 0.80 ± 0.1 nm height rP polymeric domains decreased.

**Electrochemical Characterization.** *d($TG_4T$) Redox Behavior in $Na^+$ Ions Containing Solution.* The redox behavior of d($TG_4T$) was studied by DP voltammetry in solutions of 3.0 $\mu$M d($TG_4T$) in 0.1 M sodium phosphate buffer pH = 7.0, during different incubation times (Figure 3A). Between measurements, the GCE surface was always cleaned by polishing to avoid misleading results from the d($TG_4T$) adsorption.

DP voltammograms obtained in solutions of d($TG_4T$) freshly prepared (Figure 3A black line, 0 h) and after 24 h incubation (Figure 3A, black dashed line), showed the occurrence of only the G oxidation peak, at $E_{pa}$ = +0.90 V, corresponding to the oxidation of guanine residues at the $C_8$−H position, in a two-step mechanism involving four electron and four proton transfer.[33] This is in agreement with the adsorption of only d($TG_4T$) single-strands observed in the AFM as rP random polymeric structures (Figure 1A).

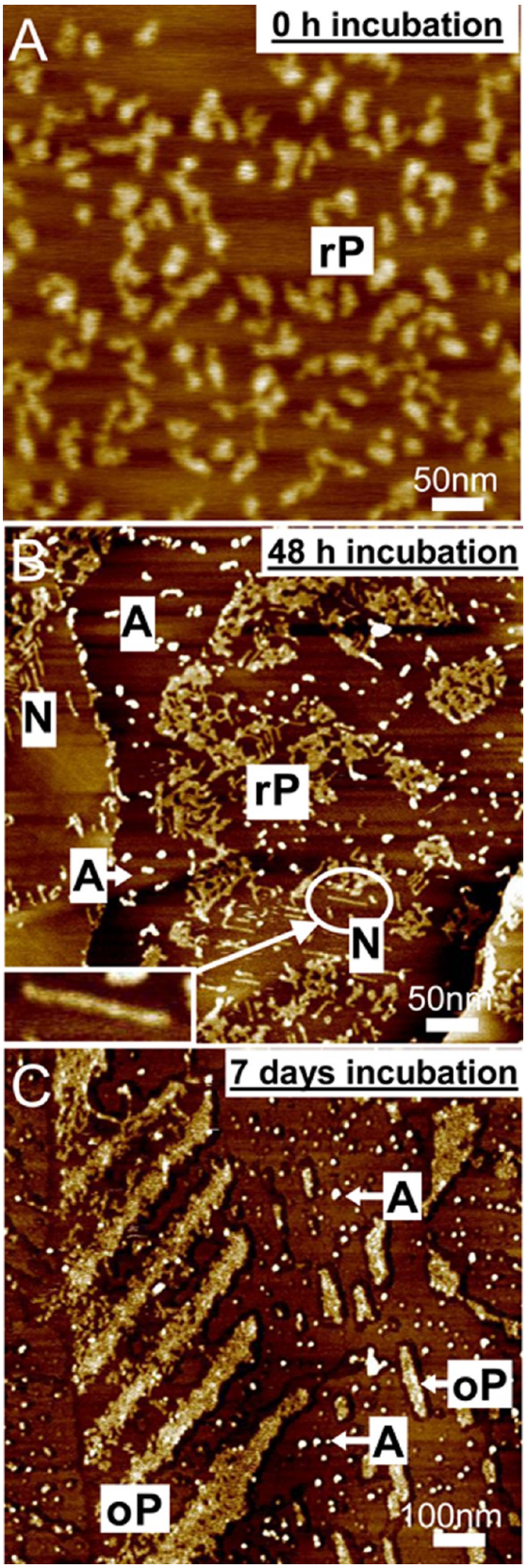


**Figure 1.** AFM images of d($TG_4T$) spontaneous adsorbed onto HOPG from 0.3 $\mu$M d($TG_4T$) in sodium phosphate buffer pH = 7.0, after (A) 0 h, (B) 72 h, and (C) 7 days incubation.


dx.doi.org/10.1021/ac500624z | Anal. Chem. XXXX, XXX, XXX−XXX

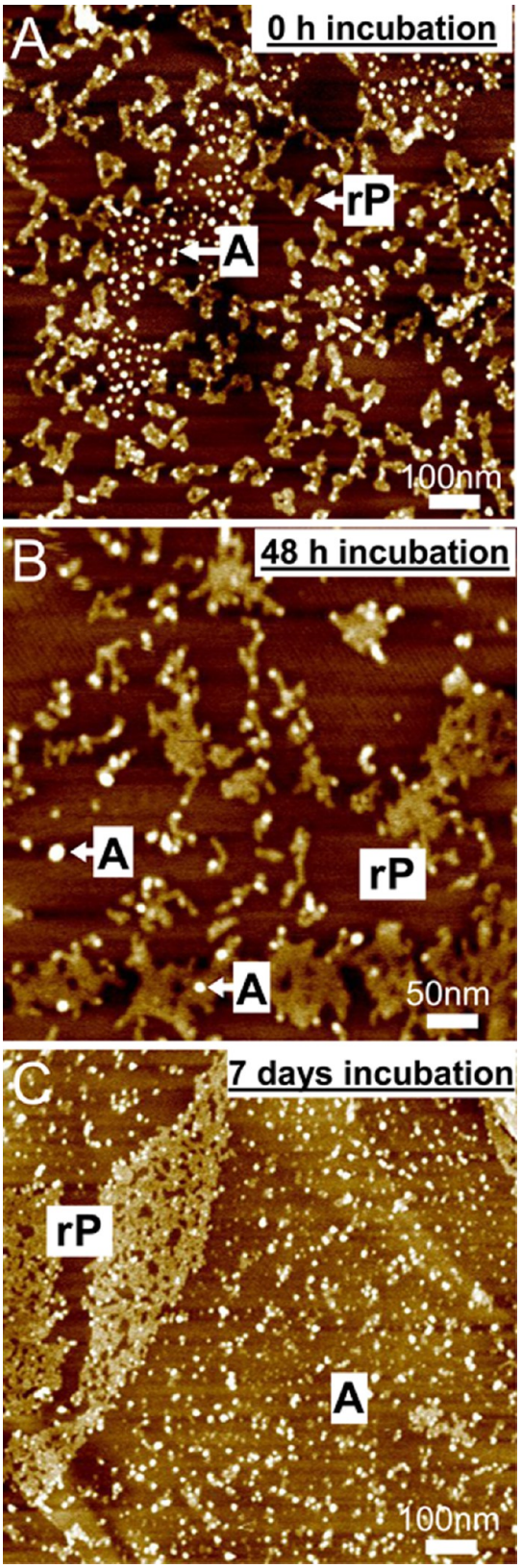


**Figure 2.** AFM images of d($TG_4T$) spontaneous adsorbed onto HOPG from 0.3 $\mu$M d($TG_4T$) in sodium phosphate buffer pH = 7.0, in the presence of 100 mM $K^+$ ions, after (A) 0 h, (B) 48 h, and (C) 7 days incubation.

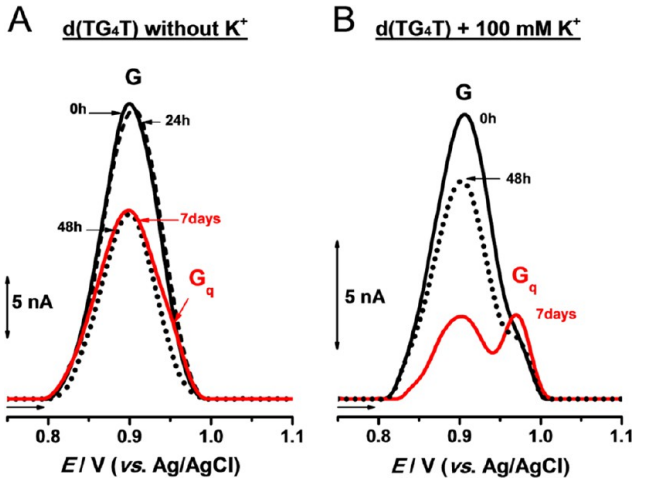


**Figure 3.** DP voltammograms baseline corrected in 3.0 $\mu$M d($TG_4T$) in sodium phosphate buffer pH = 7.0: (A) in the absence of $K^+$ ions (black line) 0 h, (black dashed line) 24 h, (black dotted line) 48 h, and (red line) 7 days incubation and (B) in the presence of 100 mM $K^+$ ions (blac line) 0 h, (black dashed line) 24 h, (black dotted line) 48 h, and (red line) 7 days incubation.

DP voltammograms obtained in the same solutions after 48 h (Figure 3A, black dotted line) and 72 h incubation also showed only the G oxidation peak that decreased with increasing the incubation time. DP voltammograms obtained after 7 days incubation (Figure 3A, red line) showed the G oxidation peak, at $E_{pa}$ = +0.90 V, due to the guanine residues in d($TG_4T$) single-strands, and a $G_q$ oxidation peak shoulder, at $E_{pa}$ = +0.95 V because of the oxidation of guanine residues in the G-quartets occurred.

*d($TG_4T$) Redox Behavior in $K^+$ Ions Containing Solution.* The d($TG_4T$) voltammetric behavior and incubation time dependence in the presence of 100 mM $K^+$ ions is shown in Figure 3B. Immediately after the addition of $K^+$ ions (Figure 3B, black line, 0 h incubation), the DP voltammograms showed both the G oxidation peak, at $E_{pa}$ = +0.91 V, due to the oxidation of guanine residues in the d($TG_4T$) single-strands, and a small $G_q$ oxidation peak shoulder, at $E_{pa}$ = +0.99 V, due to the oxidation of guanine residues in the G-quartets. A decrease of the G oxidation peak current, when compared with G oxidation peak current obtained in only $Na^+$ ions solution was observed (Figure 3A, black line). An increase of the incubation time with $K^+$ ions led to the G oxidation peak current decrease and $G_q$ oxidation peak current increase (Figure 3B, black dotted line, 48 h, and Figure 3B, red line, 7 days).

In another experiment, d($TG_4T$) was incubated with different concentrations of $K^+$ ions, during different periods of time, Figure 4. The dependence of the d($TG_4T$) voltammetric behavior on the $K^+$ ions concentration was observed after 0 h (Figure 4A), 48 h (Figure 4B), and 7 days (Figure 4C) incubation. The variation of the G oxidation peak (Figure 5A) and $G_q$ oxidation peak (Figure 5B) currents followed a similar dependence on $K^+$ ions concentration after 0 h and 7 days incubation.

DP voltammograms obtained in freshly prepared solutions (0 h incubation) of d($TG_4T$) incubated with 100 $\mu$M $K^+$ ions showed the occurrence of only G oxidation peak, at $E_{pa}$ = +0.90 V (Figure 4A, black line), and a current decrease was observed when compared with what was obtained in only $Na^+$ ions solution (Figure 4A, red dotted line). The G oxidation peak current decrease showed that even for $K^+$ ions small concentration, d($TG_4T$) started already to form G-quartets, but


dx.doi.org/10.1021/ac500624z | Anal. Chem. XXXX, XXX, XXX−XXX

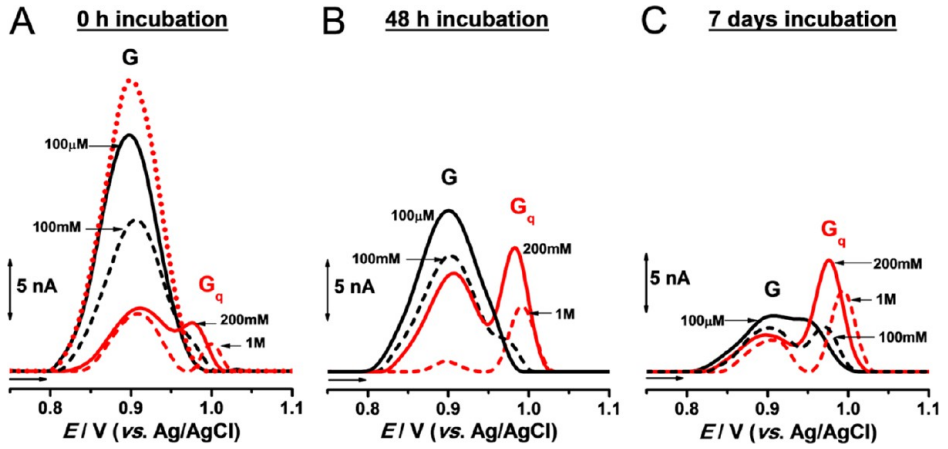


**Figure 4.** DP voltammograms baseline corrected in 3.0 $\mu$M d($TG_4T$) in sodium phosphate buffer pH = 7.0, after (A) 0 h, (B) 24 h, (C) 48 h, and (D) 7 days incubation (A, red dotted line) in the absence of $K^+$ ions and in the presence of (black line) 100 $\mu$M, (black dashed line) 100 mM, (red line) 200 mM, and (red dashed line) 1 M $K^+$ ions.

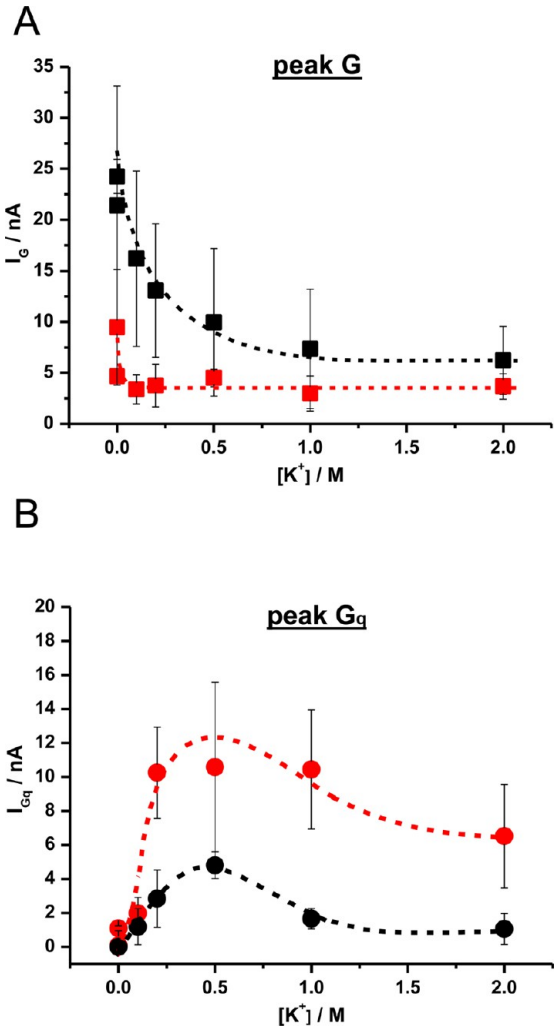


**Figure 5.** Plots of the $I_{pa}$ as a function of the concentration of $K^+$ ions: (A) peak G after (black filled square) 0 h and (red filled square) 7 days incubation, and (B) peak $G_q$ after (black filled circle) 0 h and (red filled circle) 7 days incubation.

the $G_q$ oxidation peak current was not measured because it was very small and below the DP voltammetry detection limit.

A larger decrease of the G oxidation peak current was observed for 100 mM $K^+$ ions (Figure 4A, black dashed line), and a small $G_q$ oxidation peak occurred, at $E_{pa}$ = +0.99 V, because of the oxidation of guanine residues in the G-quartets. An increase of the $K^+$ ions to 200 mM (Figure A, red line) and 500 mM $K^+$ ions caused the G oxidation peak current decrease and the $G_q$ oxidation peak current increase. For concentrations of 1 M (Figure 4A, red dashed line) and 2 M $K^+$ ions, a good separation of the $G_q$ oxidation peak, at $E_{pa}$ = +1.00 V, and a slight decrease of the $G_q$ oxidation peak current occurred.

For all $K^+$ ions concentration an increase of the incubation time to 24 h, 48 h (Figure 4B), 72 h, and 7 days (Figures 4C) led to a G oxidation peak current decrease and a $G_q$ oxidation peak current increase, when compared with 0 h incubation (Figure 4A). After 7 days incubation, the $G_q$ oxidation peak occurred even for low 100 $\mu$M $K^+$ ions (Figures 4C, black line), the $G_q$ oxidation peak current increased with increasing the $K^+$ ions up to 200 mM (Figure 4C, red line) and 500 mM $K^+$ ions. For 1 M $K^+$ ions concentration (Figure 4C, red dashed line) a good separation of the $G_q$ oxidation peak was observed, while for 2 M $K^+$ ions concentration the $G_q$ oxidation peak decreased slightly.

## DISCUSSION

The hexadeoxynucleotides d($TG_4T$) contain one block of contiguous four guanine residues and are forming parallel-stranded tetra-molecular G-quadruplexes (Scheme 1A), also stabilized by the thymine residues present at the 5′ and 3′ ends.

The AFM and voltammetric study showed d($TG_4T$) spontaneous adsorption onto HOPG (Figures 1 and 2) and oxidation at the GCE (Figures 3 and 4), with the formation and stabilization of G-quadruplexes and different higher-order nanostructures.

In $Na^+$ ions solution the formation of G-quadruplexes is a very slow process. For short incubation times (0−24 h), the d($TG_4T$) molecules remain in a single-stranded configuration, observed in AFM as rP random polymeric structures (Figure 1A) and detected by DP voltammetry by the occurrence of only the G oxidation peak (Figure 3A, black line and black dashed line, and Scheme 2). The oxidation of thymine residues in d($TG_4T$) could not be detected by DP voltammetry, because it occurs at much higher positive potential near the potential of oxygen evolution.[34]


dx.doi.org/10.1021/ac500624z | Anal. Chem. XXXX, XXX, XXX−XXX

**Scheme 2. Schematic Representation of d(TG$_4$T) Single-Stranded and Quadruplex Electrochemical Detection**

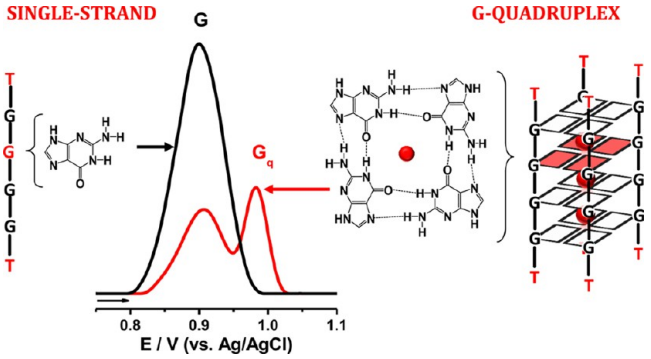


Increasing the incubation time in $Na^+$ ions solution the d(TG4T) molecules start to self-assemble into short tetra-molecular G-quadruplexes, observed in AFM as **A** spherical aggregates (Figure 1B and 1C). The d(TG4T) quadruplexes interact and adsorb less with the hydrophobic HOPG, because they have the bases protected by the sugar−phosphate backbones, when compared with the single-stranded d(TG$_4$T) molecules that have the bases more exposed and free to undergo hydrophobic interactions with the surface.[35] The d(TG$_4$T) quadruplexes were detected in DP voltammetry by the decrease of the G oxidation peak current and the occurrence of the G$_q$ oxidation peak (Figure 3A, red line, and Scheme 2). The decrease of the G oxidation peak current is due to a decrease of the concentration of guanine residues in single stranded d(TG$_4$T) and an increase of guanine residues in the tetra-molecular d(TG$_4$T) quadruplexes. The G$_q$ oxidation peak potential is higher relative to the G oxidation peak potential because of a greater difficulty for the transition of electrons from the inside of the rigid quadruplexes to the GCE surface, than from the more flexible d(TG$_4$T) single-strands.

In $Na^+$ ions solution, besides d(TG$_4$T) single-strands and quadruplexes, higher-order nanostructures could also be observed: short N nanowires for intermediate incubation times (Figure 1B) and oP oriented polymeric domains for long incubation times (Figure 1C). The nanowires and nanostructured films adsorbed on flat HOPG terraces were oriented mainly along three directions, at 60° and 120° to each other, dictated by the 3-fold symmetry of the HOPG substrate underneath.

The presence of $K^+$ ions in the solution strongly stabilizes and accelerates the G-quadruplex formation. Immediately after the addition of $K^+$ ions (0 h incubation), short tetra-molecular d(TG$_4$T) quadruplexes were formed, observed in AFM as **A** spherical aggregates (Figure 2A) and detected by DP voltammetry by the decrease of the G oxidation peak current and the occurrence of the G$_q$ oxidation peak (Figure 3B, black line, and 4A). Kinetic studies by absorbance spectroscopy of association and dissociation of tetra-molecular G-quadruplexes formed by oligonucleotides containing more than 4 contiguous guanine residues also showed faster association in the presence of $K^+$ ions.[8]

Increasing the $K^+$ ions concentration the number of adjacent G-quartets increased and were stabilized by $\pi-\pi$ hydrophobic interactions and by the presence of $K^+$, leading to the formation of a number of G-quadruplexes, confirmed by the presence of A spherical aggregates in the AFM images (Figure 2A, 100 mM $K^+$ ions, 0 h incubation).

The d(TG$_4$T) redox behavior is a time and $K^+$ ions concentration dependent process (Figure 5). After 0 h incubation, the G oxidation peak current decayed exponentially with increasing $K^+$ ions concentration until reaching a steady value (Figure 5A, black dashed line), while the G$_q$ oxidation peak current dependence on the $K^+$ ions concentration reached a maximum for 500 mM $K^+$ ion concentration (Figure 5B, black dashed line). After 7 days incubation, the G oxidation peak current reached a steady state value for all $K^+$ ions concentrations (Figure 5A, red dashed line), while the G$_q$ oxidation peak current showed a broad maximum for $K^+$ ion concentrations between 200 mM and 1 M (Figure 5B, red dashed line). At greater $K^+$ ion concentrations, above 1 M, the negative charge along the DNA backbone is screened, leading to perturbation and bending of the d(TG$_4$T) single-strands that cannot anymore form proper G-quadruplex structures, and present the electroactive centers hidden, which causes a decrease of the G$_q$ oxidation peak.

The intracellular cytoplasmic ion concentration of a typical cell is 140 mM for $K^+$ and 10 mM for $Na^+$ ions.[36] The intranuclear $K^+$ ions concentration is 3 to 8 times higher than the cytoplasmic $K^+$ ions concentration, while the intranuclear $Na^+$ ions concentration is lower than the cytoplasmic $Na^+$ ions concentration.[37] Therefore, the intracellular ionic environment, where potassium is present at high concentrations, favors the formation of tetra-molecular parallel quadruplex structures, and the intranuclear $K^+$ ion concentration of healthy cells matches the $K^+$ ion concentration interval (200 mM to 1 M) where the G$_q$ oxidation peak current reaches maximum values.

The intranuclear $Na^+/K^+$ ratio of cancer cells is altered compared with the intranuclear $Na^+/K^+$ ratio of normal cells. In cancer cells the average intranuclear $Na^+$ ions concentration increases more than 3-fold and the intranuclear $K^+$ ions concentration decreases.[38] A significant decrease of the intranuclear $K^+$ ions concentration in cancer cells can be related with a decrease of the ability of telomeric DNA to form protective G-quadruplex structures, facilitating the telomeric DNA binding and elongation by telomerase, essential for cancer cell proliferation and immortality.

## CONCLUSIONS

The transformation of the *Tetrahymena* telomeric repeat sequence d(TG$_4$T) from single-stranded into quadruplex configurations, influenced by the $Na^+$ and $K^+$ ions concentration, was successfully detected using AFM on HOPG and DP voltammetry at GCE.

The d(TG$_4$T) quadruplexes self-assembled very fast in $K^+$ ions solutions, and slowly in $Na^+$ ions solutions, revealing a time and a $K^+$ ions concentration dependent adsorption process and redox behavior. The optimum $K^+$ ions concentration for the formation of d(TG$_4$T) quadruplexes was similar to the healthy cells intracellular $K^+$ ions concentration.

The d(TG$_4$T) higher-order nanostructures self-assembled slowly in $Na^+$ ions solutions, and were detected by AFM as short nanowires and nanostructured films. The absence of higher-order nanostructures in $K^+$ ions solutions shows that the rapid formation of stable G-quadruplex structures induced by the $K^+$ ions is relevant for the good function of cells.

## AUTHOR INFORMATION

**Corresponding Author**

*E-mail: brett@ci.uc.pt.



dx.doi.org/10.1021/ac500624z | *Anal. Chem.* XXXX, XXX, XXX−XXX

## Notes

The authors declare no competing financial interest.

## ■ ACKNOWLEDGMENTS

Financial support from Fundação para a Ciência e Tecnologia (FCT), project grant (A.D.R. Pontinha), projects PTDC/SAU-BMA/118531/2010, PTDC/QEQ-MED/0586/2012, PEst-C/EME/UI0285/2013 and CENTRO-07-0224-FEDER-002001 (MT4MOBI) (cofinanced by the European Community Fund FEDER), FEDER funds through the program COMPETE—Programa Operacional Factores de Competitividade, is gratefully acknowledged.

## ■ REFERENCES

(1) Neidle, S.; Balasubramanian, S. In *Quadruplex Nucleic Acids*; Neidle, S.; Balasubramanian, S., Eds.; The Royal Society of Chemistry: Cambridge, UK, 2006.
(2) Neidle, S. In *Therapeutic Applications of Quadruplex Nucleic Acids*; Neidle, S., Ed.; Academic Press: Boston, MA, 2012; Chapter 2, pp 21—42.
(3) Punchihewa, C.; Yang, D.; In *Telomeres and Telomerase in Cancer*; Hiyama, K., Ed; Springer: New York, 2009; Chapter 11, pp 251—280.
(4) Huppert, J. L. *Biochimie* **2008**, *90*, 1140—1148.
(5) Davis, J. T.; Spada, G. P. *Chem. Soc. Rev.* **2007**, *36*, 296—313.
(6) Dapic, V.; Abdomerovic, V.; Marrington, R.; Peberdy, J.; Rodger, A.; Trent, J. O.; Bates, P. J. *Nucleic Acids Res.* **2003**, *31*, 2097—2107.
(7) Simonsson, T. *Biol. Chem.* **2001**, *382*, 621—628.
(8) Mergny, J. L.; Cian, A.; Ghelab, A.; Sacca, B.; Lacroix, L. *Nucleic Acids Res.* **2005**, *33*, 81—94.
(9) Tran, P. L.; Cian, A. D.; Gros, J.; Moriyama, R.; Mergny, J. L. *Top. Curr. Chem.* **2012**, DOI: 10.1007/128_2012_334.
(10) Aboul-Ela, F.; Murchie, A. I. H.; Lilley, D. M. J. *Nature* **1992**, *360*, 280—282.
(11) Laughlan, G.; Murchie, A. I.; Norman, D. G.; Moore, M. H.; Moody, P. C.; Lilley, D. M.; Luisi, B. *Science* **1994**, *265*, 520—524.
(12) Phillips, K.; Dauter, Z.; Murchie, A. I.; Lilley, D. M.; Luisi, B. *J. Mol. Biol.* **1997**, *273*, 171—182.
(13) Aboul-ela, F.; Murchie, A. I. H.; Norman, D. G.; Lilley, D. M. J. *J. Mol. Biol.* **1994**, *243*, 458—471.
(14) Wang, Y.; Patel, D. J. *J. Mol. Biol.* **1993**, *234*, 1171—1183.
(15) Rosu, F.; Gabelica, V.; Poncelet, H.; De Pauw, E. *Nucleic Acids Res.* **2010**, *38*, 5217—5225.
(16) Bardin, C.; Leroy, J. L. *Nucleic Acids Res.* **2008**, *36*, 477—488.
(17) Read, M. A.; Neidle, S. *Biochemistry* **2000**, *39*, 13422—13432.
(18) Clark, G. R.; Pytel, P. D.; Squire, C. J.; Neidle, S. *J. Am. Chem. Soc.* **2003**, *125*, 4066—4067.
(19) Pagano, B.; Fotticchia, I.; Tito, S.; Mattia, C. A.; Mayol, L.; Novellino, E.; Randazzo, A.; Giancola, C. *J. Nucleic Acids* **2010**, No. 247137.
(20) Marsh, T. C.; Vesenka, J.; Henderson, E. *Nucleic Acids Res.* **1995**, *23*, 696—700.
(21) Costa, L. T.; Kerkmann, M.; Hartmann, G.; Endres, S.; Bisch, P. M.; Heckl, W. M.; Thalhammer, S. *Biochem. Biophys. Res. Commun.* **2004**, *313*, 1065—1072.
(22) Neaves, K. J.; Huppert, J. L.; Henderson, R. M.; Edwardson, J. M. *Nucleic Acids Res.* **2009**, *37*, 6269—6275.
(23) Diculescu, V. C.; Chiorcea-Paquim, A.-M.; Eritja, R.; Oliveira-Brett, A. M. *J. Nucleic Acids* **2010**, No. 841932, DOI: 10.4061/2010/8419321-8.
(24) Diculescu, V. C.; Chiorcea-Paquim, A.-M.; Eritja, R.; Oliveira-Brett, A. M. *J. Electroanal. Chem.* **2011**, *656*, 159—166.
(25) Chiorcea Paquim, A. M.; Oliveira Brett, A. M. *Electrochim. Acta* **2013**, DOI: 10.1016/j.electacta.2013.07.150.
(26) Chiorcea Paquim, A. M.; Santos, P. V.; Oliveira Brett, A. M. *Electrochim. Acta* **2013**, *110*, 599—607.
(27) Chiorcea Paquim, A. M.; Santos, P. V.; Eritja, R.; Oliveira Brett, A. M. *Phys. Chem. Chem. Phys.* **2013**, *15* (23), 9117—9124.
(28) Chiorcea Paquim, A. M.; Santos, P.; Diculescu, V. C.; Eritja R.; Oliveira Brett, A. M. In *Guanine Quartets: Structure and Application*; Spada, G.P. Ed.; Royal Society of Chemistry: Cambridge, U.K., 2013; pp 100—109.
(29) McCreery, R. L. *Chem. Rev.* **2008**, *108*, 2646—2687.
(30) McDermottt, M. T.; McCreery, R. L. *Langmuir* **1994**, *10*, 4307—4314.
(31) Kang, C.; Zhang, X.; Ratliff, R.; Moyzis, R.; Rich, A. *Nature* **1992**, *356*, 126.
(32) Laughlan, G.; Murchie, A. I.; Norman, D. G.; Moore, M. H.; Moody, P. C.; Lilley, D. M.; Luisi, B. *Science* **1994**, *265*, 520.
(33) Brett, C. M. A.; Oliveira Brett, A. M.; Serrano, S. H. P. *J. Electroanal. Chem.* **1994**, *366*, 225—231.
(34) Oliveira-Brett, A. M.; Diculescu, V. C.; Chiorcea-Paquim, A.-M.; Serrano, S. H. P. In *Comprehensive Analytical Chemistry*; Alegret, S., Merkoçi, A., Eds.; Elsevier: Amsterdam, the Netherlands, 2007; Volume *49*, Chapter 20, pp 413.
(35) Chiorcea-Paquim, A.-M.; Oretskaya, T. S.; Oliveira-Brett, A. M. *Biophys. Chem.* **2006**, *121*, 131—141.
(36) Karp, G. In *Cell and Molecular Biology: Concepts and Experiments*, 6th ed.; John Wiley & Sons: Hoboken, NJ, 2009; Chapter 4, pp 153.
(37) Dick, D. A. T. *J. Physiol.* **1978**, *284*, 37—53.
(38) Nagy, I. Z.; Lustyik, G.; Nagy, V. Z.; Zarándi, B.; Bertoni-Freddari, C. *J. Cell. Biol.* **1981**, *90*, 769—777.